HHS Public Access

Author manuscript

Cell Metab. Author manuscript; available in PMC 2017 November 14.

Published in final edited form as:

Cell Metab. 2013 September 03; 18(3): 445–455. doi:10.1016/j.cmet.2013.08.006.

K_{ATP}-Channel-Dependent Regulation of Catecholaminergic Neurons Controls BAT Sympathetic Nerve Activity and Energy Homeostasis

Sulay Tovar[1,2,5], **Lars Paeger**[2,4], **Simon Hess**[2,4], **Donald A. Morgan**[6], **A. Christine Hausen**[1,2,5,9], **Hella S. Brönneke**[3], **Brigitte Hampel**[1,2,5], **P. Justus Ackermann**[1,2,5], **Nadine Evers**[1,2,5], **Hildegard Büning**[8], **F. Thomas Wunderlich**[1,2,5], **Kamal Rahmouni**[6,7], **Peter Kloppenburg**[2,4], and **Jens C. Brüning**[1,2,5,9,*]

[1]Department of Mouse Genetics and Metabolism, Institute for Genetics and Center for Molecular Medicine (CMMC), University of Cologne, Zülpicher Strasse 47b, 50674 Cologne, Germany

[2]Cologne Excellence Cluster on Cellular Stress Responses in Aging-Associated Diseases (CECAD), University of Cologne, Zülpicher Strasse 47b, 50674 Cologne, Germany

[3]Mouse Phenotyping Facility, CECAD, University of Cologne, Zülpicher Strasse 47b, 50674 Cologne, Germany

[4]Biocenter, Institute for Zoology, CMMC, University of Cologne, Zülpicher Strasse 47b, 50674 Cologne, Germany

[5]Max Planck Institute for Neurological Research, Gleueler Strasse 50, 50931 Cologne, Germany

[6]Department of Pharmacology, University of Iowa, Iowa City, IA 52242, USA

[7]Department of Internal Medicine, University of Iowa, Iowa City, IA 52242, USA

[8]Department I of Internal Medicine and CMMC, University of Cologne, Robert-Koch Strasse 21, 50931 Cologne, Germany

[9]Center for Endocrinology, Diabetes and Preventive Medicine (CEDP), University Hospital Cologne, Kerpener Strasse 62, 50924 Cologne, Germany

SUMMARY

Brown adipose tissue (BAT) is a critical regulator of glucose, lipid, and energy homeostasis, and its activity is tightly controlled by the sympathetic nervous system. However, the mechanisms underlying CNS-dependent control of BAT sympathetic nerve activity (SNA) are only partly understood. Here, we demonstrate that catecholaminergic neurons in the locus coeruleus (LC) adapt their firing frequency to extracellular glucose concentrations in a K_{ATP}-channel-dependent manner. Inhibiting K_{ATP}-channel-dependent control of neuronal activity via the expression of a variant K_{ATP} channel in tyrosine-hydroxylase-expressing neurons and in neurons of the LC enhances diet-induced obesity in mice. Obesity results from decreased energy expenditure, lower

*Correspondence: bruening@nf.mpg.de.

SUPPLEMENTAL INFORMATION

Supplemental Information contains Supplemental Experimental Procedures and four figures and can be found with this article online at http://dx.doi.org/10.1016/j.cmet.2013.08.006.

steady-state BAT SNA, and an attenuated ability of centrally applied glucose to activate BAT SNA. This impairs the thermogenic transcriptional program of BAT. Collectively, our data reveal a role of K_{ATP}-channel-dependent neuronal excitability in catecholaminergic neurons in maintaining thermogenic BAT sympathetic tone and energy homeostasis.

INTRODUCTION

Besides its prominent role in thermoregulation, recent work has revealed that brown adipose tissue (BAT) is also involved in the control of glucose and lipid metabolism in rodents (Bartelt et al., 2011; Feldmann et al., 2009; Nedergaard et al., 2011; Waldén et al., 2012). BAT function is under the control of the sympathetic nervous system (SNS). However, the regulatory mechanisms of BAT sympathetic nerve activity (SNA) in response to energy availability are still not fully understood (Richard and Picard, 2011).

Retrograde labeling with pseudorabies viruses injected into BAT of different species has allowed for the identification of neuronal populations implicated in the regulation of BAT SNA, including neurons in the rostroventrolateral medulla (RVLM), raphe pallidum (RPa), and A5 noradrenergic region as well as the locus coeruleus (LC) along with later labeling of the paraventricular hypothalamic nucleus (PVN), lateral hypothalamus (LH), and dorsomedial hypothalamus (Bamshad et al., 1999; Cano et al., 2003; Oldfield et al., 2002). Additional studies revealed robust neuroactivation in the majority of these nuclei upon cold exposure (Cano et al., 2003). Numerous studies have aimed to delineate the specific contribution of these sites to the control of thermogenesis via electrical or chemical activation or inactivation of these nuclei (Morrison, 2004; Morrison et al., 2012; Morrison et al., 2008).

In early studies, glucose was shown to induce thermogenesis when infused peripherally or directly into the CNS (Niijima, 1986; Sakaguchi and Bray, 1988). Moreover, studies revealed that intracerebroventricular (i.c.v.) injection of glucose stimulates BAT SNA and that 2-deoxyglucose inhibits BAT SNA (Egawa et al., 1989b; Holt and York, 1989a, b). These experiments indicated that glucose metabolism in neurons regulates sympathetic output to BAT and, thus, may contribute to the postprandial activation of thermogenesis. Furthermore, experiments with injections of glucose directly in nuclei from distinct areas of the hypothalamus revealed a stimulatory effect of glucose on BAT SNA when injected into the ventromedial hypothalamus (VMH), PVN, and LH, whereas, on the other hand, a stimulatory effect of glucose on BAT SNA was retained in rats with VMH lesions (Egawa et al., 1989a; Le Feuvre et al., 1991; Sakaguchi et al., 1988). Inversely, elegant studies have revealed that glucoprivation inhibits BAT thermogenesis (Egawa et al., 1989a, b), and additional studies elegantly delineated the circuitry underlying the inhibition of BAT SNA during glucose deprivation (Cao et al., 2010; Ritter et al., 1998; Madden, 2012). However, the circuitry involved in mediating the stimulatory effect of increased extracellular glucose on BAT thermogenesis, as well as the molecular mechanisms involved, remain less well defined.

Glucose-mediated neuronal excitation is partly controlled by ATP-dependent closure of potassium (K_{ATP}) channels (Jordan et al., 2010; Noma, 1983). Hence, K_{ATP} channels can

play a fundamental role as metabolic sensors because they link changes in cellular glucose metabolism to electrical activity. Notably, aside from their regulation via glucose-dependent metabolism in pancreatic β cells and neurons, cardiovascular K_{ATP} channels expressed in heart respond to other physiological stimuli than altered extracellular glucose concentrations (Suzuki et al., 2001). However, the specific role of K_{ATP} channels, which are widely expressed in defined neuronal populations (Thomzig et al., 2005) that control energy homeostasis, is only partly understood. K_{ATP} channels exhibit a wide expression pattern in the CNS, particularly clustering in a broad range of catecholaminergic neurons, including areas which control sympathetic outflow to BAT (Dunn-Meynell et al., 1998). Thus, the aim of the present study was to determine a potential function of K_{ATP} channels in catecholaminergic neurons in mediating the effect of glucose sensing on energy homeostasis.

RESULTS

Kir6.2 Is Expressed in Catecholaminergic Cells

Because previous experiments have indicated the presence of K_{ATP} channels in tyrosine hydroxylase (TH)-positive neurons (Dunn-Meynell et al., 1998; Thomzig et al., 2005), we used TH-IRES-Cre transgenic (TH-Cre) mice to genetically mark TH-positive cells and, ultimately, alter Kir6.2 function in this neuronal population (Lindeberg et al., 2004). Immunohistochemical analyses revealed the coexpression of endogenous TH with TH-Cre-dependent expression of β-galactosidase in the arcuate nucleus (ARC), PVN, dopaminergic ventral tegmental area, LC, and RVLM (Figure 1A, Figure S1A available online). Furthermore, the colocalization of Kir6.2 and TH in these regions was confirmed by immunohistochemical analysis of TH-Cre-dependent GFP expression and Kir6.2 immunoreactivity in immediately neighboring sections of these regions (Figures 1B and S1B). Altogether, Kir6.2, which can act as metabolic sensor, is expressed in the majority of catecholaminergic TH-positive neurons.

Generation of Kir6.2$^{TH\text{-}Cre}$ Mice

To directly address the functional role of Kir6.2 in TH-positive catecholaminergic neurons, we used a K_{ATP} channel variant (Kir6.2[K185Q,DN30]) that renders K_{ATP} channels resistant to closure by ATP, thereby disrupting the ability of increasing glucose concentrations to increase neuronal activity (Koster et al., 2000; Parton et al., 2007; Remedi et al., 2009). We crossed TH-Cre mice with those allowing for Cre-mediated expression of the variant Kir6.2 subunit (Kir6.2$^{TH\text{-}Cre}$ mice) (Figure S2A).

Enhanced Diet-Induced Obesity in Kir6.2$^{TH\text{-}Cre}$ Mice

Monitoring body weight of control and Kir6.2$^{TH\text{-}Cre}$ mice both under normal chow diet conditions (ND) and after exposure to a high-fat diet (HFD) revealed a slight increase in body weight of the Kir6.2$^{TH\text{-}Cre}$ mice in comparison to controls upon exposure to ND (Figure 1C). Importantly, we had previously demonstrated that TH-Cre mice on the same C57BL/6 genetic background did not exhibit alterations in body weight or energy homeostasis (Könner et al., 2011). Interestingly, the difference in body weight was more apparent when the animals were exposed to HFD (Figure 1D). Furthermore, obesity in

Kir6.2$^{TH\text{-}Cre}$ mice was confirmed by the relative increase in fat mass and epididymal fat pad weight under both ND and HFD conditions (Figures 1E, 1F, and S2B) as well as by significant hyperleptinemia in Kir6.2$^{TH\text{-}Cre}$ mice on HFD (Figure S2C). Finally, morphological analysis of white adipose tissue (WAT) revealed hyperplasia of adipocytes in the Kir6.2$^{TH\text{-}Cre}$ mice (Figures 1G and 1H).

The assessment of food intake and energy expenditure by indirect calorimetry in control and Kir6.2$^{TH\text{-}Cre}$ mice on HFD revealed no significant change in food intake of Kir6.2$^{TH\text{-}Cre}$ mice on HFD (Figure 2A). In contrast, energy expenditure was significantly reduced in these animals (Figure 2B). On the other hand, energy content in feces and food efficiency remained unaltered in Kir6.2$^{TH\text{-}Cre}$ mice on HFD (Figure S2D). Collectively, decreased energy expenditure rather than increased food intake may account for the exacerbated obesity in Kir6.2$^{TH\text{-}Cre}$ mice.

We also determined blood glucose and plasma insulin concentrations, which showed hyperglycemia and hyperinsulinemia in HFD-fed Kir6.2$^{TH\text{-}Cre}$ mice in comparison to controls (Figures S2E and S2F). Kir6.2$^{TH\text{-}Cre}$ mice exhibited slightly impaired glucose tolerance and slightly impaired insulin tolerance, even under ND conditions (Figures S2G and S2H). Moreover, HFD-mediated impairment in glucose tolerance, but not insulin sensitivity, was significantly enhanced in Kir6.2$^{TH\text{-}Cre}$ mice (Figures S2G and S2H). Collectively, the expression of the variant Kir6.2 subunit in TH neurons impairs glucose tolerance as well as insulin sensitivity even under ND conditions, and this effect was enhanced when these animals were exposed to HFD.

Reduced Sympathetic Outflow to BAT in Kir6.2$^{TH\text{-}Cre}$ Mice

To further define the underlying mechanism of enhanced sensitivity to obesity and impairment of glucose metabolism in Kir6.2$^{TH\text{-}Cre}$ mice, we assessed the morphology of BAT. Although BAT of control mice exhibited the normal appearance of multivacuolar brown adipocytes (Figure 2C, upper panel), the histomorphological characteristics of brown adipocytes in Kir6.2$^{TH\text{-}Cre}$ mice had a rather macrovacuolar, white-adipocyte-like phenotype (Figure 2C, lower panel). Moreover, BAT of Kir6.2$^{TH\text{-}Cre}$ mice exhibited slightly reduced messenger RNA expression of the brown adipocyte differentiation marker *Cidea*, *Ppargc1a*, and *Ucp1* as key regulators of mitochondrial biogenesis and uncoupling (Figure 2D). Moreover, protein expression of UCP1 in BAT of Kir6.2$^{TH\text{-}Cre}$ mice in comparison to controls was reduced (Figure 2E).

Given that BAT function is tightly regulated by the SNS and that sympathetic denervation of BAT has been shown to result in similar histomorphological changes, as observed in Kir6.2$^{TH\text{-}Cre}$ mice (Minokoshi et al., 1986), we measured BAT SNA in control and Kir6.2$^{TH\text{-}Cre}$ mice. This analysis revealed a significant reduction in BAT SNA in Kir6.2$^{TH\text{-}Cre}$ mice in comparison to controls (Figure 2F). In contrast, adrenal SNA (Figure 2G) and SNA of inguinal WAT (Figure S3A) remained unaltered in these animals, which was consistent with unaltered circulating plasma epinephrine and norepinephrine concentrations (Figures S3B and S3C). Moreover, the regulation of heart rate and blood pressure in Kir6.2$^{TH\text{-}Cre}$ mice remained unaltered (Figures 2H and 2I). Restrain stress

induced serum corticosterone concentrations in Kir6.2$^{TH\text{-}Cre}$ mice and controls to a similar extent (Figure S3D).

Centrally Applied Glucose Fails to Increase BAT SNA in Kir6.2$^{TH\text{-}Cre}$ Mice

Next, we assessed BAT SNA response to i.c.v. injection of glucose. Although glucose increased BAT SNA by almost 4-fold in control mice, this response was largely attenuated in Kir6.2$^{TH\text{-}Cre}$ mice (Figures 2J and 2K). Thus, K_{ATP}-channel-dependent neuronal excitability of TH-expressing neurons is critical for centrally applied glucose to activate BAT SNA.

Next, we monitored body temperature in control and Kir6.2$^{TH\text{-}Cre}$ mice during exposure to 4°C, revealing that, after cold exposure, Kir6.2$^{TH\text{-}Cre}$ mice had a reduced body core temperature (Figure 2L). In summary, the expression of an ATP-insensitive Kir6.2 subunit in catecholaminergic neurons of mice results in obesity and reduced sympathetic outflow to BAT as well as an inability to increase BAT SNA in response to centrally applied glucose, resulting in an appropriate thermogenic response under cold conditions.

TH-Positive Neurons in the Locus Coeruleus Are Responsive to Glucose

Retrograde tracing experiments had demonstrated that sympathetic innervation of BAT arises from a neurocircuitry including the PVN, RVLM, and RPa as well as the LC (Bamshad et al., 1999; Cano et al., 2003; Oldfield et al., 2002). K_{ATP}-dependent regulation of neuronal activity indicates glucose responsiveness (Miki and Seino, 2005), and neurons in these regions express not only the Kir6.2 subunit (Figures 1B and S1B) but also glucokinase, a key regulator of the glucose-sensing machinery (Lynch et al., 2000). Because the major regulatory neurons in control of sympathetic innervation, which are located in the RVLM, have been shown to be glucose inhibited (Madden, 2012), we sought to identify TH-positive neurons, which are glucose activated. Thus, we investigated the response of LC neurons to variant glucose concentrations. Comparing action potential frequency in noradrenergic LC neurons of control and Kir6.2$^{TH\text{-}Cre}$ mice revealed a reduced firing frequency of LC neurons in Kir6.2$^{TH\text{-}Cre}$ mice in comparison to controls (Figures 3A and 3B). Decreasing extracellular glucose concentrations from 5 to 3 mM led to a decrease in firing frequency and membrane hyperpolarization in ~ 40% of LC neurons in control mice (Figure 3C); a response that could be reversed via blocking K_{ATP} channels through the application of the K_{ATP} channel blocker tolbutamide (Figure 3C). Out of all neurons recorded under this condition (n = 30), we also found two glucose-inhibited neurons (data not shown). Consistent with the role of K_{ATP} channels in the glucose-mediated regulation of LC neurons, the glucose responsiveness of these cells was abolished in Kir6.2$^{TH\text{-}Cre}$ mice (Figures 3D and 3E). Conversely, increasing glucose concentrations from 5 to 8 mM increased the firing of a subset of LC neurons in control mice; an effect that was absent in LC neurons of Kir6.2$^{TH\text{-}Cre}$ mice (Figures 3F–3H). Altogether, TH-positive neurons in the LC respond to alterations in extracellular glucose concentrations with concomitant changes in firing properties in a K_{ATP}-channel-dependent manner.

K_{ATP}-Dependent Control of LC Neurons Regulates BAT SNA

Thus, we directly addressed the potential functional role of K_{ATP}-channel-dependent regulation of LC neuron excitability on energy homeostasis in vivo. For this purpose, we

performed bilateral stereotactic injections of recombinant adeno-associated viral vectors (AAVs) expressing either GFP or Cre into the LC of Rosa26$^{Kir6.2}$ mice (Figure 4A). Immunohistochemical staining of brain sections from these animals with a GFP antibody revealed the successful targeting of the LC (Figure 4B). Monitoring of body weight revealed an increase in body weight of mice that had been injected with AAV-Cre in comparison to those injected with AAV-GFP as early as 10 days after microinjections, and this difference became most prominent 4 weeks after gene delivery (Figure 4C). Consistent with increased weight gain upon selective expression of the variant Kir6.2 subunit in the LC, these mice exhibited increased adiposity, as indicated by an elevated total body fat content (Figure 4D) and epigonadal fat pad mass (Figure 4E) as well as WAT hyperplasia (Figure 4F). BAT exhibited a similar change in histomorphological appearance as observed in Kir6.2$^{TH\text{-}Cre}$ mice (compare Figure 4G to Figure 2C), and the expression of *Ucp1* in BAT was reduced by ~50% in comparison to control mice (Figure 4G), indicative of reduced BAT SNA upon the inhibition of K_{ATP}-channel-dependent neuronal excitation specifically in the LC. Moreover, although glucose stimulated BAT SNA by 4-fold in mice that had been injected with AAV-GFP, glucose failed to activate BAT SNA when the mutant Kir6.2 subunit was expressed in the LC upon AAV-Cre injection (Figures 4H and 4I). In contrast, mice injected with AAV-Cre exhibited no difference in adrenal or renal SNA as well as in blood pressure and heart rate in comparison to controls (Figures S4A–S4C). Moreover, in comparison to mice injected with AAV-GFP, mice that received AAV-Cre microinjections into the LC exhibited an impaired cold tolerance (Figure 4J). Altogether, glucose-elicited, K_{ATP}-channel-dependent control of neuronal activity of LC neurons contributes to the regulation of BAT SNA as well as adaptive responses to high-fat feeding in order to maintain energy homeostasis.

DISCUSSION

Our current understanding of both the neuronal circuitry that controls BAT SNA and the cellular mechanisms adapting this activity to the nutrient availability of the organism is still incomplete. Numerous elaborate studies have revealed a role for hypothalamic centers, which receive information about the energy availability of the organism and, in part, directly respond to varying extracellular glucose concentrations in control of BAT SNA outflow via brainstem centers (Morrison et al., 2012; Richard and Picard, 2011). Particularly, the ability of centrally applied glucose to stimulate BAT SNA has been intensely studied (Egawa et al., 1989a, b; Holt and York, 1989a, b; Madden, 2012).

Retrograde tracing from BAT had indicated that the neurons labeled from BAT to large proportion represent TH-positive sympathetic premotor neurons, such as those located in the RVLM and RPa and also TH-positive neurons in the PVN, and these sites have been shown to exhibit the activation of cFos expression upon cold exposure, a condition for promoting BAT SNA (Cano et al., 2003; Miyata et al., 1995). Indeed, a series of elegant studies by Morrison et al., 2012, 2008, and others has clearly established a critical role for these neurons in control of sympathetic innervation of BAT. TH expression in these sites clearly overlaps with the expression of Kir6.2 (Dunn-Meynell et al., 1998). Therefore, the experiments provided in the current study establish that K_{ATP}-channel-dependent control of neuronal excitability in catecholaminergic neurons controls BAT SNA and that this

regulation is required for the control of energy and glucose homeostasis. The attenuated ability of centrally applied glucose to activate BAT SNA may stem from direct impairment of glucose sensing in the sympathetic premotor neurons in the RVLM, RPa, or the intermediolateral nucleus (IML). At least Kir6.2-dependent, glucose-mediated neuronal activation in the RVLM appears unlikely, given that it has been demonstrated that RVLM-neurons are activated by glucoprivation and that this, in turn, activates GABAergic innervation of the RPa in order to inhibit BAT SNA. Nevertheless, we cannot rule out that the abrogation of Kir6.2-mediated control of RPa, IML, or other catecholaminergic neurons may contribute to the obese phenotype of Kir6.2$^{TH\text{-}Cre}$ mice.

Interestingly, aside from the neurons directly implied in control of BAT SNA, the largest catecholaminergic cell group in the CNS—namely, the LC—has been identified by retrograde tracing from BAT, although at later stages of infection with rabies viruses (Cano et al., 2003). Nevertheless, c-Fos immunoreactivity in the LC is activated within 3 to 24 hr of cold exposure, and bilateral lesions of the LC cause obesity in monkeys (Miyata et al., 1995; Redmond et al., 1977). These experiments pointed toward the possibility that neurons in the LC modulate BAT SNA. This is unlikely to be controlled via direct stimulation of sympathetic premotor neurons, given that the LC clearly acts as a center for integrating information of sympathetic stimuli (Samuels and Szabadi, 2008a). It serves critical functions in adapting higher brain functions such as arousal, cognitive performance, and autonomic output to sensory input from the periphery of the organism. However, in addition to these widespread cortical projections, the LC provides also catecholaminergic innervation to key regulatory centers of BAT SNA, including the sympathetic premotor neurons in the RVLM and RPa (Samuels and Szabadi, 2008a, b; Tanaka et al., 1996). It was also demonstrated that the ability of neuropeptide Y-expressing neurons in the ARC to regulate BAT thermogenesis coincides with an altered sympathetic output via TH neurons in the PVN and LC (Shi et al., 2013). Interestingly, LC projections have been demonstrated to inhibit RVLM neurons, which, in turn, provide inhibitory input to RPa neurons (Samuels and Szabadi, 2008a; Van Bockstaele et al., 1989). On the other hand, projections from the LC to the RPa are likely to have excitatory effects via alpha1-adrenoreceptor activation (Samuels and Szabadi, 2008a). Collectively, the glucose-evoked activation of the LC potentially inhibits RVLM neurons to disinhibit RPa neurons in control of BAT SNA. This would be in line with a general view that catecholaminergic innervation serves rather a modulatory effect for adapting the precision and threshold of neuronal activation. Nevertheless, the attenuation of glucose-evoked activation of BAT SNA upon the inhibition of K_{ATP}-channel-dependent neuroactivation in the LC points to an unrecognized modulatory role for TH neurons in the LC for controlling BAT SNA and energy homeostasis. This may be of clinical relevance, given that LC neurons are also subject to neurodegeneration in diseases such as Alzheimer's and Parkinson's (Del Tredici and Braak, 2013). Thus, LC neuron loss may contribute to altered autonomic innervation and, ultimately, to metabolic disturbances associated with these neurodegenerative disorders.

EXPERIMENTAL PROCEDURES

Animal Care

All animal procedures and euthanasia were reviewed by the animal care committee of the University of Cologne, approved by local government authorities (Bezirksregierung Köln), and performed in accordance with National Institutes of Health guidelines. Mouse husbandry was performed as previously described (Könner et al., 2007).

Generation of Kir6.2$^{TH\text{-}Cre}$ Mice

TH-IRES-Cre mice (Lindeberg et al., 2004) were mated with Rosa26-$^{Kir6.2}$[K185Q, ΔN30] mice (Remedi et al., 2009), and breeding colonies were maintained by mating homozygous ROSA26$^{Kir6.2}$ mice with TH-IRES-Cre mice in order to obtain Kir6.2$^{TH\text{-}Cre}$ mice and the respective controls.

Analysis of Body Composition

Nuclear magnetic resonance (NMR) was employed in order to determine the whole-body composition of live animals with the minispec mq7.5 NMR Analyzer (Bruker Optik).

Immunohistochemistry

Free-floating coronal sections were cut at 25 μm through the ARC, PVN, ventrotegmental area, substantia nigra, LC, and RVLM from paraformaldehyde-fixed brains with a freezing microtome (Leica), and sections were subsequently stained with the indicated antibodies (detailed information can be found in the Supplemental Experimental Procedures).

Electrophysiology

Perforated patch clamp recordings were performed as previously described (Könner et al., 2011). For detailed information, see the Supplemental Experimental Procedures.

In Vivo AAV Injections

Homozygous Rosa26$^{Kir6.2}$ mice (8 weeks of age, exposed to HFD from 3 weeks of age on) were anesthetized and positioned in a Stoelting stereotaxic frame, and a bilateral injection with AAV-Cre or AVV-GFP into the LC was performed.

Statistical Methods

Data sets were analyzed for statistical significance with a two-tailed unpaired student's t test unless stated otherwise. All p values below 0.05 were considered significant. All displayed values are means ± SEM. *$p \leq 0.05$, **$p \leq 0.01$, and ***$p \leq 0.001$ versus controls. Statistic analysis for food intake was performed in relation to body weight, and energy expenditure was analyzed with an applied general linear model and analysis of covariance (R software, http://www.r-project.org).

Supplementary Material

Refer to Web version on PubMed Central for supplementary material.

Acknowledgments

We wish to thank G. Schmall and T. Rayle for excellent secretarial assistance and P. Scholl, S. Irlenbusch, J. Goldau, J. Alber, H. Janicki, and H. Wratil for outstanding technical assistance. We thank T. Ebendal for providing TH-IRES-Cre mice and J. Samulski (University of North Carolina, Chapel Hill) for providing pXX6-80. This work was supported by the Center for Molecular Medicine Cologne, the University of Cologne (TVA1 to J.C.B., D7 to P.K., and B5 to H.B.), the European Union (FP7-HEALTH-2009-241592, EurOCHIP, to J.C.B.), the DFG (BR 1492/7-1 to J.C.B.; KL 762/2-2 and KL 762/4-1 to P.K.), the Competence Network for Adipositas (Neurotarget) funded by the Federal Ministry of Education and Research (FKZ01GIO845 to J.C.B.), the National Institutes of Health (HL084207 to K.R.), the American Diabetes Association (1-11-BS-127 to K.R.), and the Humboldt foundation (to S.T.).

References

Bamshad M, Song CK, Bartness TJ. CNS origins of the sympathetic nervous system outflow to brown adipose tissue. Am J Physiol. 1999; 276:R1569–R1578. [PubMed: 10362733]

Bartelt A, Bruns OT, Reimer R, Hohenberg H, Ittrich H, Peldschus K, Kaul MG, Tromsdorf UI, Weller H, Waurisch C, et al. Brown adipose tissue activity controls triglyceride clearance. Nat Med. 2011; 17:200–205. [PubMed: 21258337]

Cano G, Passerin AM, Schiltz JC, Card JP, Morrison SF, Sved AF. Anatomical substrates for the central control of sympathetic outflow to interscapular adipose tissue during cold exposure. J Comp Neurol. 2003; 460:303–326. [PubMed: 12692852]

Cao WH, Madden CJ, Morrison SF. Inhibition of brown adipose tissue thermogenesis by neurons in the ventrolateral medulla and in the nucleus tractus solitarius. Am J Physiol Regul Integr Comp Physiol. 2010; 299:R277–R290. [PubMed: 20410479]

Del Tredici K, Braak H. Dysfunction of the locus coeruleus-norepinephrine system and related circuitry in Parkinson's disease-related dementia. J Neurol Neurosurg Psychiatry. 2013; 84:774–783. [PubMed: 23064099]

Dunn-Meynell AA, Rawson NE, Levin BE. Distribution and phenotype of neurons containing the ATP-sensitive K+ channel in rat brain. Brain Res. 1998; 814:41–54. [PubMed: 9838037]

Egawa M, Yoshimatsu H, Bray GA. Effects of 2-deoxy-D-glucose on sympathetic nerve activity to interscapular brown adipose tissue. Am J Physiol. 1989a; 257:R1377–R1385. [PubMed: 2603998]

Egawa M, Yoshimatsu H, Bray GA. Lateral hypothalamic injection of 2-deoxy-D-glucose suppresses sympathetic activity. Am J Physiol. 1989b; 257:R1386–R1392. [PubMed: 2603999]

Feldmann HM, Golozoubova V, Cannon B, Nedergaard J. UCP1 ablation induces obesity and abolishes diet-induced thermogenesis in mice exempt from thermal stress by living at thermoneutrality. Cell Metab. 2009; 9:203–209. [PubMed: 19187776]

Holt SJ, York DA. Interaction of intracerebroventricular insulin and glucose in the regulation of the activity of sympathetic efferent nerves to brown adipose tissue in lean and obese Zucker rats. Brain Res. 1989a; 500:384–388. [PubMed: 2691017]

Holt SJ, York DA. Studies on the sympathetic efferent nerves of brown adipose tissue of lean and obese Zucker rats. Brain Res. 1989b; 481:106–112. [PubMed: 2706453]

Jordan SD, Könner AC, Brüning JC. Sensing the fuels: glucose and lipid signaling in the CNS controlling energy homeostasis. Cell Mol Life Sci. 2010; 67:3255–3273. [PubMed: 20549539]

Könner AC, Janoschek R, Plum L, Jordan SD, Rother E, Ma X, Xu C, Enriori P, Hampel B, Barsh GS, et al. Insulin action in AgRP-expressing neurons is required for suppression of hepatic glucose production. Cell Metab. 2007; 5:438–449. [PubMed: 17550779]

Könner AC, Hess S, Tovar S, Mesaros A, Sánchez-Lasheras C, Evers N, Verhagen LA, Brönneke HS, Kleinridders A, Hampel B, et al. Role for insulin signaling in catecholaminergic neurons in control of energy homeostasis. Cell Metab. 2011; 13:720–728. [PubMed: 21641553]

Koster JC, Marshall BA, Ensor N, Corbett JA, Nichols CG. Targeted overactivity of beta cell K(ATP) channels induces profound neonatal diabetes. Cell. 2000; 100:645–654. [PubMed: 10761930]

Le Feuvre RA, Woods AJ, Stock MJ, Rothwell NJ. Effects of central injection of glucose on thermogenesis in normal, VMH-lesioned and genetically obese rats. Brain Res. 1991; 547:110–114. [PubMed: 1860063]

Lindeberg J, Usoskin D, Bengtsson H, Gustafsson A, Kylberg A, Söderström S, Ebendal T. Transgenic expression of Cre recombinase from the tyrosine hydroxylase locus. Genesis. 2004; 40:67–73. [PubMed: 15452869]

Lynch RM, Tompkins LS, Brooks HL, Dunn-Meynell AA, Levin BE. Localization of glucokinase gene expression in the rat brain. Diabetes. 2000; 49:693–700. [PubMed: 10905475]

Madden CJ. Glucoprivation in the ventrolateral medulla decreases brown adipose tissue sympathetic nerve activity by decreasing the activity of neurons in raphe pallidus. Am J Physiol Regul Integr Comp Physiol. 2012; 302:R224–R232. [PubMed: 22071154]

Miki T, Seino S. Roles of KATP channels as metabolic sensors in acute metabolic changes. J Mol Cell Cardiol. 2005; 38:917–925. [PubMed: 15910876]

Minokoshi Y, Saito M, Shimazu T. Metabolic and morphological alterations of brown adipose tissue after sympathetic denervation in rats. J Auton Nerv Syst. 1986; 15:197–204. [PubMed: 3958437]

Miyata S, Ishiyama M, Shido O, Nakashima T, Shibata M, Kiyohara T. Central mechanism of neural activation with cold acclimation of rats using Fos immunohistochemistry. Neurosci Res. 1995; 22:209–218. [PubMed: 7566702]

Morrison SF. Central pathways controlling brown adipose tissue thermogenesis. News Physiol Sci. 2004; 19:67–74. [PubMed: 15016906]

Morrison SF, Nakamura K, Madden CJ. Central control of thermogenesis in mammals. Exp Physiol. 2008; 93:773–797. [PubMed: 18469069]

Morrison SF, Madden CJ, Tupone D. Central control of brown adipose tissue thermogenesis (Lausanne: Front Endocrinol). 2012:3.

Nedergaard J, Bengtsson T, Cannon B. New powers of brown fat: fighting the metabolic syndrome. Cell Metab. 2011; 13:238–240. [PubMed: 21356513]

Niijima A. Effect of glucose and other hexoses on efferent discharges of brown adipose tissue nerves. Am J Physiol. 1986; 251:R240–R242. [PubMed: 3740304]

Noma A. ATP-regulated K+ channels in cardiac muscle. Nature. 1983; 305:147–148. [PubMed: 6310409]

Oldfield BJ, Giles ME, Watson A, Anderson C, Colvill LM, McKinley MJ. The neurochemical characterisation of hypothalamic pathways projecting polysynaptically to brown adipose tissue in the rat. Neuroscience. 2002; 110:515–526. [PubMed: 11906790]

Parton LE, Ye CP, Coppari R, Enriori PJ, Choi B, Zhang CY, Xu C, Vianna CR, Balthasar N, Lee CE, et al. Glucose sensing by POMC neurons regulates glucose homeostasis and is impaired in obesity. Nature. 2007; 449:228–232. [PubMed: 17728716]

Redmond DE Jr, Huang YH, Snyder DR, Maas JW, Baulu J. Hyperphagia and hyperdipsia after locus coeruleus lesions in the stumptailed monkey. Life Sci. 1977; 20:1619–1628. [PubMed: 406491]

Remedi MS, Kurata HT, Scott A, Wunderlich FT, Rother E, Kleinridders A, Tong A, Brüning JC, Koster JC, Nichols CG. Secondary consequences of beta cell inexcitability: identification and prevention in a murine model of K(ATP)-induced neonatal diabetes mellitus. Cell Metab. 2009; 9:140–151. [PubMed: 19187772]

Richard D, Picard F. Brown fat biology and thermogenesis. Front Biosci (Landmark Ed). 2011; 16:1233–1260. [PubMed: 21196229]

Ritter S, Llewellyn-Smith I, Dinh TT. Subgroups of hindbrain catecholamine neurons are selectively activated by 2-deoxy-D-glucose induced metabolic challenge. Brain Res. 1998; 805:41–54. [PubMed: 9733914]

Sakaguchi T, Bray GA. Sympathetic activity following paraventricular injections of glucose and insulin. Brain Res Bull. 1988; 21:25–29. [PubMed: 3064881]

Sakaguchi T, Bray GA, Eddlestone G. Sympathetic activity following paraventricular or ventromedial hypothalamic lesions in rats. Brain Res Bull. 1988; 20:461–465. [PubMed: 3293706]

Samuels ER, Szabadi E. Functional neuroanatomy of the noradrenergic locus coeruleus: its roles in the regulation of arousal and autonomic function part I: principles of functional organisation. Curr Neuropharmacol. 2008a; 6:235–253. [PubMed: 19506723]

Samuels ER, Szabadi E. Functional neuroanatomy of the noradrenergic locus coeruleus: its roles in the regulation of arousal and autonomic function part II: physiological and pharmacological

manipulations and pathological alterations of locus coeruleus activity in humans. Curr Neuropharmacol. 2008b; 6:254–285. [PubMed: 19506724]

Shi YC, Lau J, Lin Z, Zhang H, Zhai L, Sperk G, Heilbronn R, Mietzsch M, Weger S, Huang XF, et al. Arcuate NPY controls sympathetic output and BAT function via a relay of tyrosine hydroxylase neurons in the PVN. Cell Metab. 2013; 17:236–248. [PubMed: 23395170]

Suzuki M, Li RA, Miki T, Uemura H, Sakamoto N, Ohmoto-Sekine Y, Tamagawa M, Ogura T, Seino S, Marbán E, Nakaya H. Functional roles of cardiac and vascular ATP-sensitive potassium channels clarified by Kir6.2-knockout mice. Circ Res. 2001; 88:570–577. [PubMed: 11282890]

Tanaka M, Matsumoto Y, Murakami T, Hisa Y, Ibata Y. The origins of catecholaminergic innervation in the rostral ventromedial medulla oblongata of the rat. Neurosci Lett. 1996; 207:53–56. [PubMed: 8710209]

Thomzig A, Laube G, Prüss H, Veh RW. Pore-forming subunits of K-ATP channels, Kir6.1 and Kir6.2, display prominent differences in regional and cellular distribution in the rat brain. J Comp Neurol. 2005; 484:313–330. [PubMed: 15739238]

Van Bockstaele EJ, Pieribone VA, Aston-Jones G. Diverse afferents converge on the nucleus paragigantocellularis in the rat ventrolateral medulla: retrograde and anterograde tracing studies. J Comp Neurol. 1989; 290:561–584. [PubMed: 2482306]

Waldén TB, Hansen IR, Timmons JA, Cannon B, Nedergaard J. Recruited vs. nonrecruited molecular signatures of brown, “brite,” and white adipose tissues. Am J Physiol Endocrinol Metab. 2012; 302:E19–E31. [PubMed: 21828341]

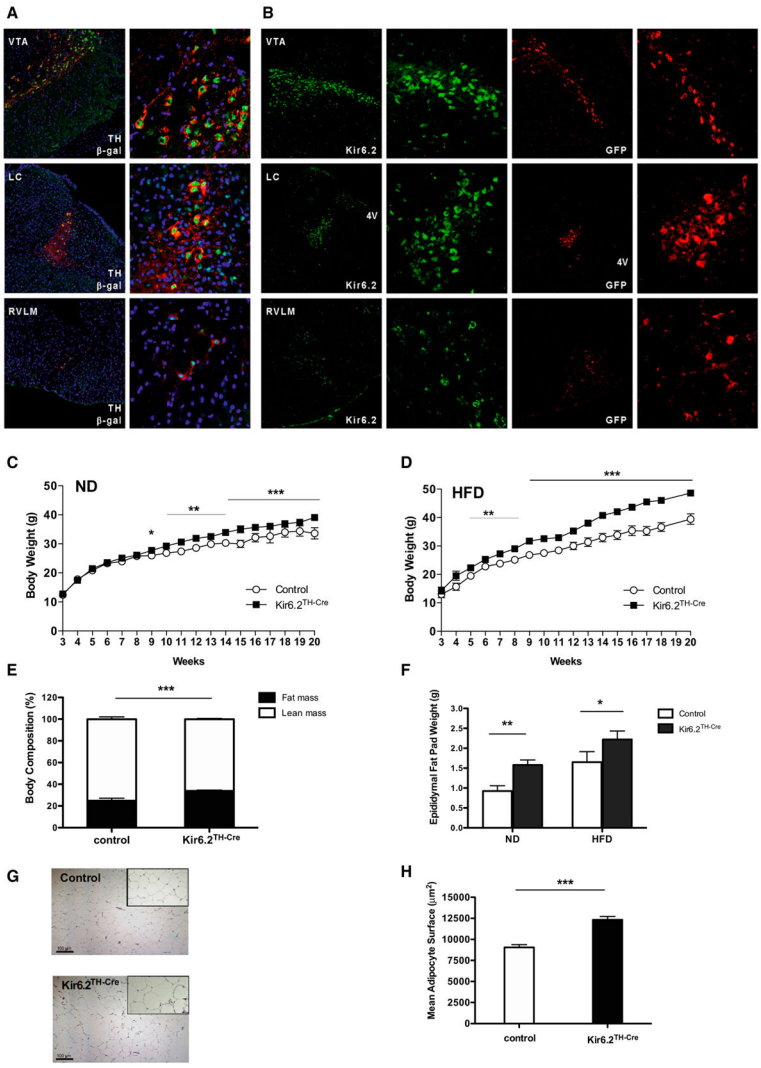

Figure 1. Kir6.2$^{TH\text{-}Cre}$ Mice Develop Diet-Induced Obesity

(A) Visualization of Cre activity in TH-IRES-Cre-LacZ reporter mice. Double immunofluorescence for endogenous TH and transgenically expressed β-galactosidase (β-gal) in different brain regions of double-heterozygous TH-IRES-Cre-LacZ reporter mice is also shown. Nuclear staining, blue (DAPI); β-gal staining, green; tyrosine hydroxylase, red (TH). Ventral tegmental area, VTA; locus coeruleus, LC; rostroventrolateral medulla, RVLM. Details are shown at a higher magnification.

(B) Expression of Kir6.2 in catecholaminergic neurons. Immunofluorescence detection of Kir6.2 expression and GFP in adjacent sections of double heterozygous TH-IRES-Cre-GFP reporter mice is also shown. TH-IRES-Cre-negative littermates were used as controls. Green, Kir6.2; red, GFP. Details are shown at a higher magnification.

(C) Average body weight of male control (n = 14) and Kir6.2$^{TH\text{-}Cre}$ mice (n = 18) on normal chow diet (ND).

(D) Average body weight of male control (n = 12) and Kir6.2$^{TH\text{-}Cre}$ mice (n = 12) on high-fat diet (HFD).

(E) Average body fat content of 20-week-old male control (n = 13) and Kir6.2$^{TH\text{-}Cre}$ mice (n = 14) on HFD measured by nuclear magnetic resonance.
(F) Epididymal fat pad weight of 20-week-old male control and Kir6.2$^{TH\text{-}Cre}$ mice on ND (control, n = 12; Kir6.2$^{TH\text{-}Cre}$, n = 15) and on HFD (control, n = 13; Kir6.2$^{TH\text{-}Cre}$, n = 14).
(G) Representative H&E staining of epididymal adipose tissue of a 20-week-old male control (upper panel) and Kir6.2$^{TH\text{-}Cre}$ mice (lower panel) on HFD (10× magnification in the small square).
(H) Quantification of mean adipocyte surface in epididymal adipose tissue of 20-week-old male control (n = 4) and Kir6.2$^{TH\text{-}Cre}$ mice (n = 4) on HFD.
Data are expressed as mean ± SEM. *$p < 0.05$, **$p < 0.01$, and ***$p < 0.001$ between control and Kir6.2$^{TH\text{-}Cre}$ mice. See also Figures S1 and S2.

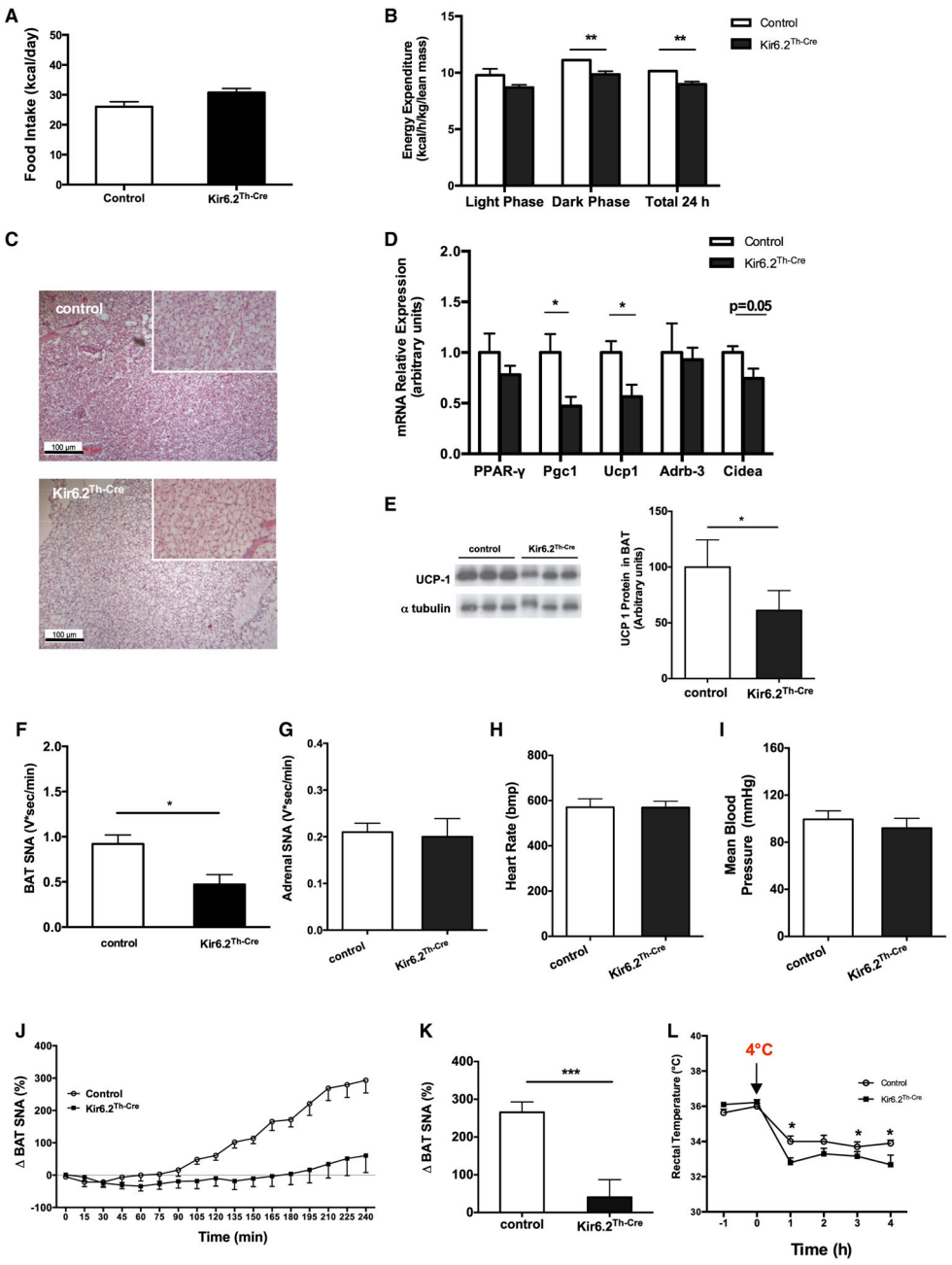

Figure 2. Impaired BAT SNA in Kir6.2$^{TH\text{-}Cre}$ Mice

(A) Average daily food intake of 15-week-old male control (n = 12) and Kir6.2$^{TH\text{-}Cre}$ mice (n = 14) on HFD.

(B) Energy expenditure corrected for lean body mass of 20-week-old male control (n = 12) and Kir6.2$^{TH\text{-}Cre}$ mice (n = 13) on HFD.

(C) Representative hematoxylin and eosin (H&E) staining of BAT of a 20-week-old male control (upper panel) and Kir6.2$^{TH\text{-}Cre}$ mice (lower panel) on HFD (10× magnification in the small square).

(D) Relative expression of peroxisome proliferator-activated receptor γ (*Pparg* [PPAR-γ]), peroxisome proliferator-activated receptor coactivator 1α (*Ppargc1a* [Pgc1]), uncoupling protein 1 (*Ucp1*), β3-adrenergic receptor (*Adrb3*), and cell-death-inducing DFF45-like effector protein a (*Cidea*) in BAT extracts from 20-week-old control (n = 6) and Kir6.2$^{TH\text{-}Cre}$ mice (n = 6) on HFD.

(E) Immunoblot analysis (left) and quantification (right) of UCP1 protein expression in BAT of 20-week-old control and Kir6.2$^{TH\text{-}Cre}$ mice on HFD. α-tubulin was used as a loading control.

(F) Quantification of BAT SNA of 15-week-old control (n = 5) and Kir6.2$^{TH\text{-}Cre}$ mice (n = 5) on HFD.

(G) Adrenal SNA in 15-week-old control (n = 6) and Kir6.2$^{TH\text{-}Cre}$ mice (n = 6) on HFD.

(H and I) Heart rate and mean arterial pressure in control (n = 4) and Kir6.2$^{TH\text{-}Cre}$ mice (n = 5) measured in fully awake and unrestrained mice.

(J) BAT SNA response induced by i.c.v. glucose injection in control (n = 8) and Kir6.2$^{TH\text{-}Cre}$ mice (n = 5) on HFD.

(K) A comparison of BAT SNA responses induced by i.c.v. glucose injection (an average of the last hour of recording) between control and Kir6.2$^{TH\text{-}Cre}$ mice.

(L) Rectal temperature of 15-week-old control (n = 6) and Kir6.2$^{TH\text{-}Cre}$ mice (n = 6) on HFD upon cold exposure (+4°C) for 4 hr.

Data are expressed as mean ± SEM. *p < 0.05, **p < 0.01, and ***p < 0.001 between control and Kir6.2$^{TH\text{-}Cre}$ mice. See also Figure S3.

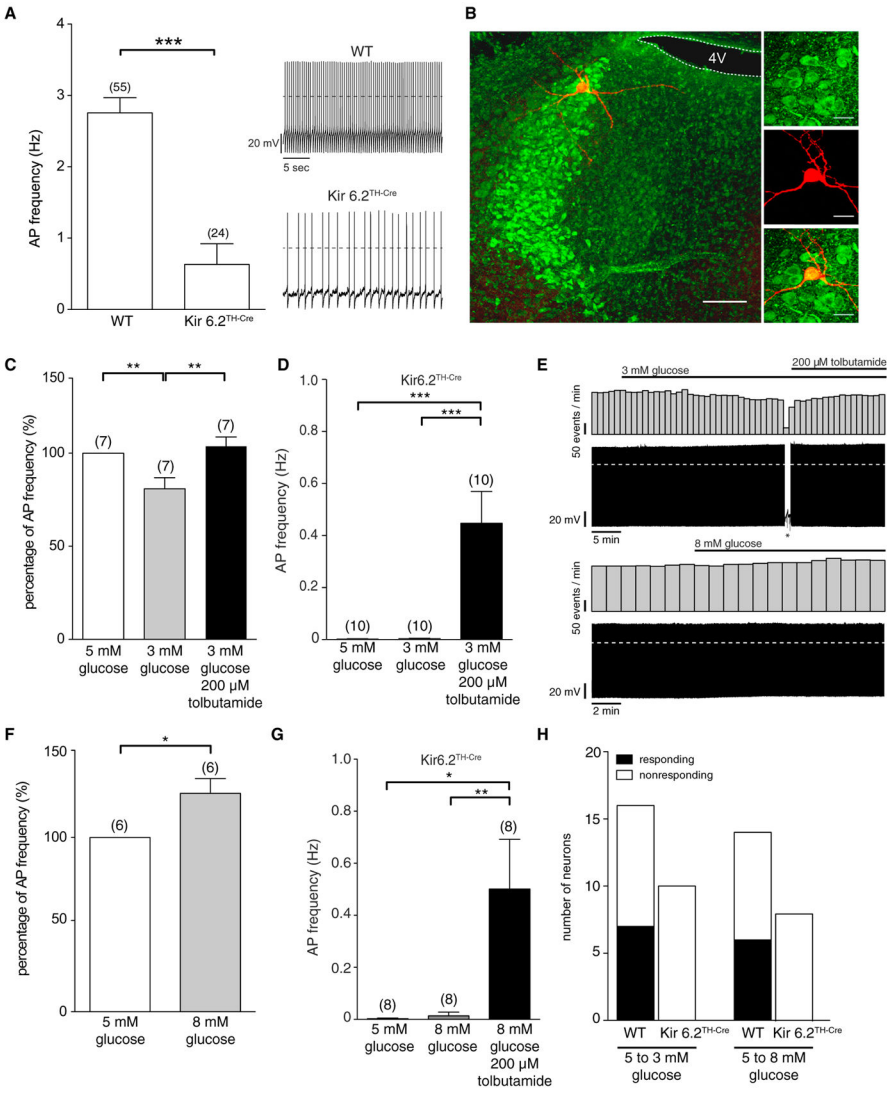

Figure 3. Glucose Responses of LC Neurons in Control and Kir6.2$^{TH\text{-}Cre}$ Mice

(A) Perforated patch clamp recordings of LC neurons in male control (C57BL/6 and TH-Cre-negative Kir6.2 littermates) and Kir6.2$^{TH\text{-}Cre}$ mice. Basal firing frequency is reduced in neurons expressing the mutant Kir6.2 subunit.

(B) Antibody staining of dopamine-β-hydroxylase (green) and recorded single neuron backfilled with biocytin-confirming location in the LC (left, the scale bar represents 100 µM; right, the scale bar represents 25 µM).

(C) Relative reduction of action potential (AP) frequency induced by a decreased extracellular glucose concentration (5 to 3 mM) and after an increase in frequency by the application of 200 µM tolbutamide.

(D) LC neurons of Kir6.2$^{TH\text{-}Cre}$ mice show no changes in AP frequency upon varying glucose concentrations but show increased firing upon tolbutamide application.

(E) A reduction of extracellular glucose concentration (5 to 3 mM) reduces AP frequency, which is reversed by the application of 200 µM tolbutamide (upper panel, the asterisk marks

current injection protocols). An increase of extracellular glucose (5 to 8 mM) concentration leads to an increase of AP frequency of control LC neurons (lower panel).
(F) Relative increase of AP frequency by increasing extracellular glucose (5 to 8 mM) in control LC neurons.
(G) LC neurons of Kir6.2$^{TH\text{-}Cre}$ mice show no changes in AP frequency upon an increase of extracellular glucose concentration but show increased firing upon tolbutamide application.
(H) The number of neurons in LC that respond to an increase and decrease of extracellular glucose concentration in control and Kir6.2$^{TH\text{-}Cre}$ mice.
Data are expressed as mean ± SEM. *$p < 0.05$, **$p < 0.01$, and ***$p < 0.001$. Counts (n) are expressed in the figure.

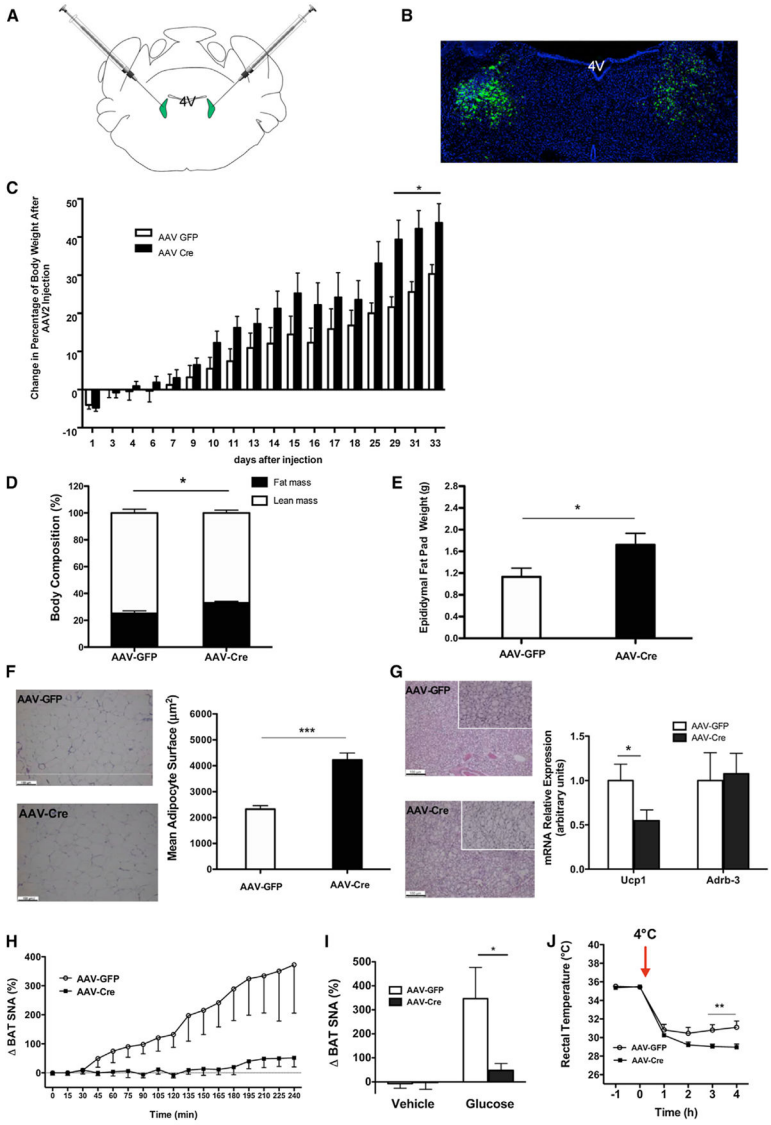

Figure 4. K_{ATP} Channels in the LC Control BAT Function and Energy Homeostasis

(A) A schematic representation showing the localization of AAV injection. AAV expressing either GFP or Cre was injected into the LC of Rosa26$^{Kir6.2}$ mice (anteroposterior, ~5.45; mediolateral, ± 1.28; dorsoventral, 3.65).

(B) Representative photomicrographs depicting GFP -immunoreactivity (green, GFP; blue, DAPI nuclear staining) from Rosa26$^{Kir6.2}$ mice bilaterally injected with AAV-GFP vectors into the LC.

(C) Change of body weight after bilateral LC injection of AAV-GFP (n = 6) or AAV-Cre (n = 8). Rosa26$^{Kir6.2}$ mice exposed to HFD from 3 weeks of age on were injected with the respective AAV vectors at the age of 8 weeks, and body weight was followed for another 4 weeks. Change of body weight after AAV vector injection is expressed as a percentage the difference from preinjection body weight.

(D) Body composition (% lean and fat mass) of mice expressing the mutant form of Kir6.2 specifically in LC (AAV-Cre) (n = 8) versus control (AAV-GFP) (n = 6) 7 weeks after AAV vector injection measured by NMR.
(E) Increased epididymal fat pad weight in mice expressing the mutant form of Kir6.2 specifically in LC (AAV-Cre) (n = 7) versus control (AAV-GFP) (n = 6) 7 weeks after AAV vector injection.
(F) Representative H&E staining of epididymal adipose tissue (left) of a 15-week-old male control mice (AAV-GFP; upper panel) and AAV-Cre mice (lower panel) on HFD. Quantification of mean adipocyte surface in epididymal adipose tissue of 20-week-old male control (AAV-GFP, n = 6) and AAV-Cre mice (n = 6) on HFD (right).
(G) Representative H&E staining of BAT (left) of a 15-week-old male control (AAV-GFP, upper panel) and AAV-Cre (lower panel) mice on HFD (10× magnification in the small square). The relative expression of uncoupling protein 1 (*Ucp1*) and β3-adrenergic receptor (*Adrb3*) in BAT extracts of control (AAV-GFP, n = 5) and AAV-Cre mice (n = 7) on HFD (right). The expression of indicated messenger RNAs was normalized to that of *Hprt*, and the resultant value for each group was normalized to the expression of the target gene in control mice.
(H) Time course of BAT SNA response induced by i.c.v. glucose (100 nM) in HFD-fed Rosa26$^{Kir6.2}$ mice that received either AAV-GFP (n = 6) or AAV-Cre (n = 6) into the LC.
(I) A comparison of BAT SNA responses after i.c.v. injection of vehicle or glucose between HFD-fed Rosa26$^{Kir6.2}$ mice that received either AAV-GFP (vehicle, n = 3; glucose, n = 6) or AAV-Cre (vehicle, n = 3; glucose, n = 6) into the LC.
(J) Rectal temperature of AAV-GFP (n = 5) and AAV-Cre microinjected mice (n = 8) on HFD upon cold exposure (+4°C).
Data are expressed as mean ± SEM. *$p < 0.05$ and **$p < 0.01$ between control (AAV-GFP) versus AAV-Cre mice. See also Figure S4.